

Tissue Probability Map Constrained CLASSIC for Increased Accuracy and Robustness in Serial Image Segmentation

Zhong Xue^a, Dinggang Shen^b and Stephen TC Wong^a

^aThe Center for Biotechnology and Informatics, The Methodist Hospital Research Institute and Department of Radiology, The Methodist Hospital, Weill Cornell Medical College, Houston, TX; ^bDepartment of Radiology and Biomedical Research Imaging Center, University of North Carolina, Chapel Hill, NC

ABSTRACT

Traditional fuzzy clustering algorithms have been successfully applied in MR image segmentation for quantitative morphological analysis. However, the clustering results might be biased due to the variability of tissue intensities and anatomical structures. For example, clustering-based algorithms tend to over-segment white matter tissues of MR brain images. To solve this problem, we introduce a tissue probability map constrained clustering algorithm and apply it to serial MR brain image segmentation for longitudinal study of human brains. The tissue probability maps consist of segmentation priors obtained from a population and reflect the probability of different tissue types. More accurate image segmentation can be achieved by using these segmentation priors in the clustering algorithm. Experimental results of both simulated longitudinal MR brain data and the Alzheimer's Disease Neuroimaging Initiative (ADNI) data using the new serial image segmentation algorithm in the framework of CLASSIC show more accurate and robust longitudinal measures.

1. INTRODUCTION

Image segmentation plays an important role in quantitative analysis of MR brain images of many medical imaging applications, such as automatic tissue labeling and quantification, morphometry, image registration, and image-guided surgery.¹⁻³ In longitudinal image computing, it is important to quantify the subtle morphological changes of MR brain images for better understanding or earlier detection of neurological diseases. In these studies, a series of 3-D images of the same subject are usually captured at different timepoints, and the focus is to quantitatively measure the morphological changes of the whole brain or a specific regions^{4,5} across with time. Therefore, longitudinal stability is critical since the temporal changes in these applications are usually subtle and the true signal of morphological information might be overwhelmed by the measurement errors if we process the serial images individually. It is in this context that existing 3-D segmentation and registration algorithms may not be able to provide sufficient power for longitudinal image computing. In addition to the measurement errors, it is also a challenge when the presence of vascular or other pathologies changes signal characteristics, *i.e.*, tissue contrast change, thereby rendering tissue segmentation unreliable. Therefore, in order to more accurately and robustly measure the temporal signal changes, it is important to accurately align longitudinally corresponding anatomical structures and measure these anatomical changes across different timepoints by using the temporal information provided in the 3-D image series.

Based on the idea of joint segmentation and registration for serial image computing,⁶⁻¹² we have proposed the CLASSIC algorithm for longitudinal MR brain image analysis.¹³ The algorithm incorporates an iterative serial image segmentation and registration strategy in order to improve the longitudinal stability for 3-D image series. It iteratively performs two steps: i) estimate the longitudinal deformations using a 4-D elastic warping algorithm,⁵ and ii) jointly segment images using a 4-D clustering algorithm based on the current estimate of the longitudinal deformations. The 4-D segmentation algorithm is based on an extension of the FANTASM

Further author information:

Zhong Xue: E-mail: zxue@tmhs.org

Dinggang Shen: E-mail: dgshen@med.unc.edu

Stephen TC Wong: Email: stwong@tmhs.org

algorithm¹⁴ by using additional temporal constraints forcing temporally corresponding voxels being segmented with the same tissue type. The 4-D elastic warping algorithm is applied to better estimate the longitudinal correspondence and segmentation iteratively. Experimental results on simulated and real longitudinal MR brain images showed both segmentation accuracy and longitudinal consistency.

Our work in this paper is based on the earlier method described above¹³ in that we use tissue probability map as an additional constraint in the fuzzy clustering algorithm. Traditional clustering methods might be biased by the tissue population and intensity differences, as well as the spatial distribution of tissues or the anatomical structures since the size and intensities of different tissue classes vary greatly in different images and applications. For example, most clustering-based algorithms tend to over-segment white matter tissues of MR brain images. To solve this problem, we introduce a tissue probability map or segmentation prior constrained clustering algorithm and apply it to serial MR brain image segmentation. The tissue probability maps consist of the segmentation priors obtained from a population and reflect the probability of a voxel belonging to different tissue types. In this way, the clustering algorithm is not only driven by the image data but also constrained by the probability of different tissue types of each image location, thus increased segmentation accuracy and robustness is obtained. We then apply the new segmentation algorithm in the framework of CLASSIC. For convenience, in the rest of this paper we refer the new algorithm as CLASSIC-II, and the method in¹³ as CLASSIC-I (with no tissue probability constraint).

Experiments are performed to segment both simulated and real longitudinal MR brain images. For the simulated images, longitudinal atrophies at the temporal lobe of each simulated subject image are introduced using the statistical model-based deformable simulation.¹⁵ Because the underlying temporal deformations and segmentations are known, the correct classification rates are calculated to quantitatively evaluate the accuracy of the proposed algorithm. Both CLASSIC-I and II are compared, and the results show that by using the tissue probability map more accurate segmentation results can be obtained. Specifically, the new algorithm overcomes the disadvantage of over-segmentation of white matter for clustering-based image segmentation. For real images, the longitudinal 3-D T1-SPGR MR images of the Alzheimer's Disease Neuroimaging Initiative (ADNI) are used in the experiments. In all the experiments, we focused on evaluating the performance of the algorithms in terms of obtaining temporally-consistent segmentation, capturing global and local intensity/contrast changes, as well as estimating longitudinal deformations.

2. METHOD

2.1 The Framework of the Algorithm

The algorithm incorporates an iterative serial image segmentation and registration strategy in order to improve the longitudinal stability for 3-D image series. It iteratively performs two steps:¹³

- Step 1: Given the current segmentation results, the algorithm refines the underlying longitudinal deformations among the serial images using the 4-D elastic image warping algorithm.⁵ Notice that other registration algorithms that take an initial deformation field and refine the registration result based on the input segmented images in order to better match them, can also be easily embedded into this framework;
- Step 2: Given a current estimate of the longitudinal deformations necessary to align serial 3-D images, the algorithm jointly segments the image series using the tissue probability map constrained 4-D clustering algorithm. The major idea is that temporal consistent segmentation is achieved for longitudinally corresponding tissues, and the use of tissue probability map constraint improves the accuracy and robustness of the image segmentation.

Fig. 1 illustrates the flowchart of this iterative algorithm. After input a series of images the initial 3-D segmentation of the serial images is performed using AdpkMean.¹⁶ Then, these segmented images can be used as the input for the 4-D elastic deformable registration,⁵ and after the longitudinal deformations among the serial images have been estimated, the proposed 4-D clustering algorithm for serial images will refine the segmentation. These 4-D registration and segmentation procedures can be performed iteratively, and the algorithm stops when the difference between two consequent iterations is smaller than a prescribed threshold.

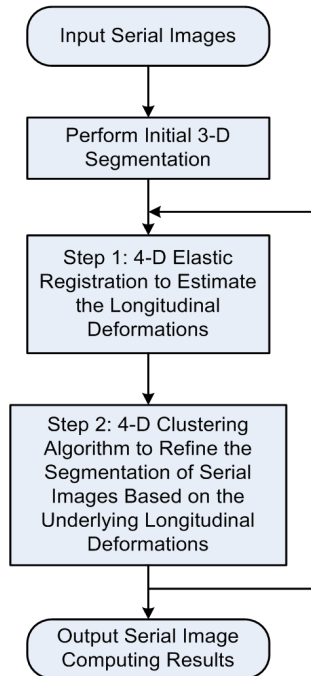


Figure 1. The flowchart of the iterative CLASSIC framework.

The algorithm of 4-D HAMMER (Shen et al⁵) is used in step 1, and it overcomes the shortcomings of using the 3-D registration independently for image warping in longitudinal study. As we know that applying 3-D method in serial images typically leads to noisy longitudinal measures. In the 4-D elastic image registration, the longitudinal deformations are estimated simultaneously. This is different from the 3-D warping methods, which aim at establishing only the deformation between two images at a time. The 4-D registration algorithm produces smooth and accurate estimations of longitudinal changes. Most importantly, morphological features and matches guiding this deformation process are determined via 4-D image analysis, which significantly reduces noise and improves robustness in detecting anatomical correspondence.

The tissue probability map-based 4-D segmentation algorithm used in step 2 is introduced in Section 2.2.

2.2 The Tissue Probability Map Constrained 4-D Clustering Algorithm

2.2.1 Tissue Probability Map Constrained 4-D Fuzzy Clustering Algorithm

In traditional clustering-based segmentation, since the size and intensities of different tissue classes vary greatly in different images and applications, the clustering results might be biased by the tissue population and intensity differences, as well as the spatial distribution of tissues or the anatomical structures. Herein, we propose to use the tissue probability map as an additional constraint of the clustering algorithm to overcome such disadvantages.

Given a series of images $I_t, t \in T, T = \{t_1, t_2, \dots, t_Y\}$ and the underlying longitudinal deformations $F_{t_1 \rightarrow t}, t = t_2, \dots, t_Y$, the goal of the 4-D segmentation is to classify the tissues into white matter (WM), gray matter (GM) and cerebrospinal fluid (CSF). The segmented images are denoted as $I_t^{(\text{seg})}, t \in T$. Since $F_{t_1 \rightarrow t}$ is the deformation from I_{t_1} to I_t , the corresponding point of a voxel i in image I_{t_1} will be point $F_{t_1 \rightarrow t}(i)$ in image I_t . For simplicity, we denote the point $F_{t_1 \rightarrow t}(i)$ in image I_t as (t, i) , thus $x_{(t,i)}$ indicates the intensity of point (t, i) .

From the segmentation results of the images of a population we can obtain the tissue probability map $p_{(t,i),k}$ and align it onto the space of the first image of the image series using HAMMER.¹⁷ The tissue probability map reflects the probability or segmentation prior of point (t, i) belonging to class k . This prior information can then be used as an additional constraint in the fuzzy clustering algorithm to reduce the effect of biased segmentation

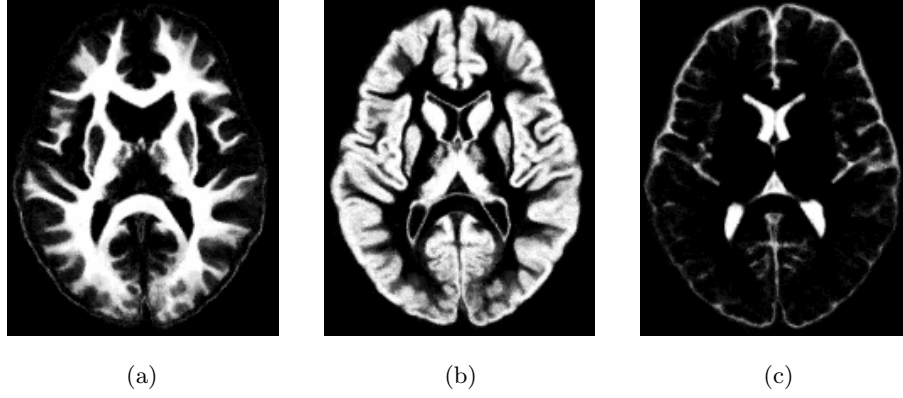


Figure 2. The tissue probability maps of different tissue types calculated from 150 images of the ADNI dataset. (a) WM map, (b) GM map, and (c) CSF map.

results. This new tissue probability map constrained 4-D clustering algorithm can be formulated by minimizing the following objective function:

$$E(\mu, c) = \frac{1}{2} \sum_{t \in T} \sum_{i \in \Omega} \sum_{k=1}^K \{ \mu_{(t,i),k}^2 (x_{(t,i)} - c_{t,k})^2 + \gamma (\mu_{(t,i),k} - p_{(t,i),k})^2 + \alpha \mu_{(t,i),k}^2 \bar{\mu}_{(t,i),k}^{(s)} + \beta \mu_{(t,i),k}^2 \bar{\mu}_{(t,i),k}^{(t)} \}, \quad (1)$$

where voxel $x_{(t,i)}$ ($t \in T, i \in \Omega$) is classified into different tissue types by finding the clustering centers $c_{t,k}$, the k th clustering center of image I_t , and $\mu_{(t,i),k}$, the fuzzy membership function of $x_{(t,i)}$ belonging to class k . Ω is the image domain of I_t . K is the number of tissue types. The first term in Eq.(1) is the standard energy term for fuzzy clustering algorithm. The second term reflects the constraint of the tissue probability map and γ is the weight for the constraint. The third and the fourth terms are the spatial segmentation consistency and the temporal segmentation consistency constraints along the longitudinal deformations, respectively. α and β are the weights for these two constraints.

$$\bar{\mu}_{(t,i),k}^{(s)} = \frac{1}{N_1} \sum_{(t,i) \in N_{(t,i)}^{(s)'}} \sum_{m \in M_k} \mu_{(t,i),m}^2,$$

and

$$\bar{\mu}_{(t,i),k}^{(t)} = \frac{1}{N_2} \sum_{(t,i) \in N_{(t,i)}^{(t)'}} \sum_{m \in M_k} \mu_{(t,i),m}^2,$$

where $N_{(t,i)}^{(s)}$ is the spatial neighborhood of point (t, i) , and

$$N_{(t,i)}^{(t)} = \{(\tau, i) : |\tau - t| \leq T_N\}$$

is the temporal neighborhood of point (t, i) along the temporal deformation, and N_1 and N_2 are the normalization factors. T_N is the size of the temporal neighborhood, and $M_k = \{l : k = 1, \dots, K, \text{ and } l \neq k\}$. The fuzzy membership functions are subject to

$$\sum_{k=1}^K \mu_{(t,i),k} = 1, \text{ for all } i \in \Omega, t \in T. \quad (2)$$

It can be seen that the algorithm becomes the segmentation step in the CLASSIC-I (with no spatial adaptation for clustering centers) when $\gamma = 0$, it is similar to the Robust FCM algorithm¹⁴ when $\gamma = 0$ and $\beta = 0$, and

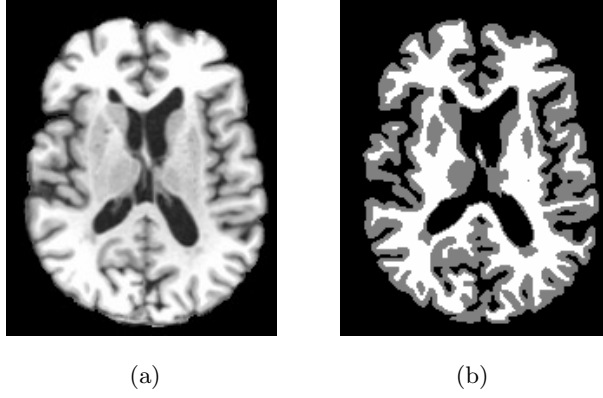


Figure 3. The template image. (a) the template image, (b) the segmentation of the template image.

it becomes the standard FCM algorithm when $\alpha = 0, \beta = 0$, and $\gamma = 0$. Therefore, by setting properly the parameters α , β , and γ , we can apply constraints on spatial smoothness, temporal consistency, and prior tissue knowledge on the 4-D clustering algorithm.

Using Lagrange multipliers to enforce the constraint Eq.(2) in Eq.(1), and calculating its partial derivatives with respect to μ and c , we can get the equations to iteratively update them:

$$\mu_{(t,i),k} = \left(\frac{1 - \sum_{l=1}^K \{\gamma p_{(t,i),l} g_{(t,i),l}^{-1}\}}{\sum_{l=1}^K g_{(t,i),l}^{-1}} + \gamma p_{(t,i),k} \right) \cdot g_{(t,i),k}^{-1}, \quad t \in T, \quad i \in \Omega, \quad (3)$$

where

$$g_{(t,i),k} = (x_{(t,i)} - c_{t,k})^2 + \gamma + \alpha \bar{\mu}_{(t,i),k}^{(s)} + \beta \bar{\mu}_{(t,i),k}^{(t)},$$

and

$$c_{t,k} = \frac{\sum_{i \in \Omega} \mu_{(t,i),k}^2 x_{(t,i)}}{\sum_{i \in \Omega} \mu_{(t,i),k}^2}. \quad (4)$$

The 4-D clustering algorithm can be summarized as follows:

- Step (1): Set α , β , γ , and neighborhoods $N_{(t,i)}^{(s)}$, $N_{(t,i)}^{(t)}$, and T_N , and compute fuzzy membership functions using Eq.(3);
- Step (2): compute clustering centroids using Eq.(4);
- Step (3): if the algorithm converges (the difference of the values of the objective function between two iterations is smaller than a prescribed threshold), output the segmentation results, otherwise go back to step (1).

Similar to the standard FCM algorithm, the new algorithm usually converges after 10 to 20 iterations dependent on the difference values to terminate the iteration. This serial image segmentation algorithm is used in Step 2 of the CLASSIC framework as described in Section 2.1.

The tissue probability map is calculated from the segmentation results of a population, *i.e.*, all the S sample images captured from a population are first segmented using a 3-D segmentation algorithm¹⁶ and then aligned onto the space of the template image I_{temp} using¹⁷. Denoting $n^{\text{temp}}(i, k)$ as the number of aligned sample images whose voxel i is segmented as tissue k , the segmentation prior of class k at voxel i is defined as,

$$p_{i,k}^{\text{temp}} = \frac{n^{\text{temp}}(i, k)}{S}, \quad i \in \Omega_{\text{temp}}, \quad k = 1, \dots, K, \quad (5)$$

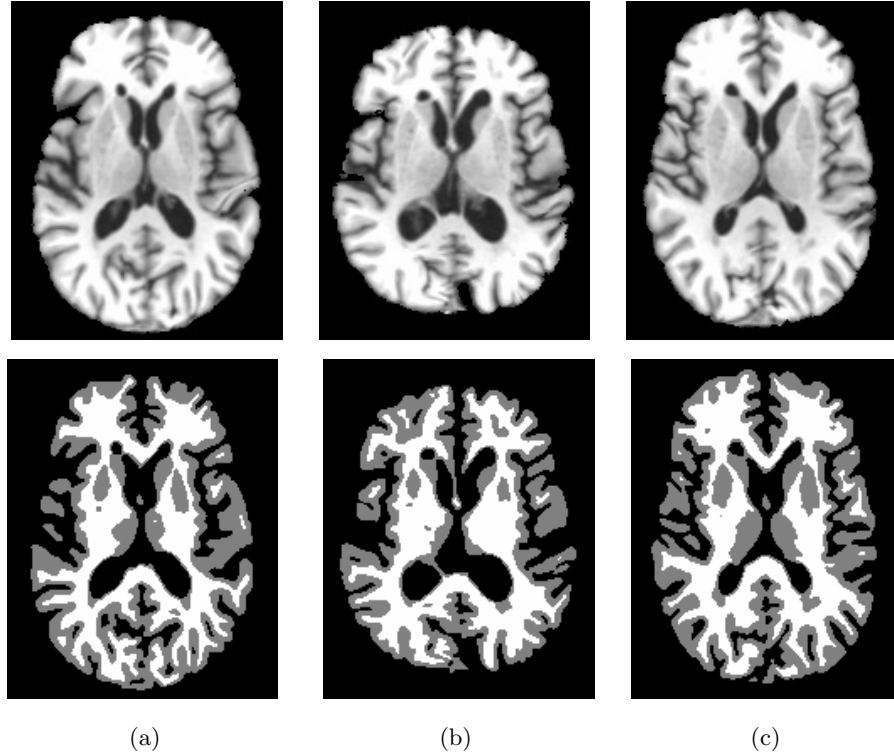


Figure 4. Three simulated images. Top: simulated T1-weighted images, bottom: simulated segmentation images.

where Ω_{temp} is the space of the template image, and $\sum_{k=1}^K p_{i,k}^{\text{temp}} = 1$. When applying the segmentation prior onto a series of input images $I_t, t = t_1, \dots, t_Y$, we can transform the segmentation prior $p_{i,k}^{\text{temp}}$ onto the space of the first image I_{t_1} . Herein, the HAMMER program¹⁷ is applied to align all the segmentation results onto the template image space, as well as to transfer the template image onto the first timepoint image. We denote the transformed prior in the first timepoint image domain as $p_{(t,i),k}$, which is used in Eq.(1) as the tissue probability map. Fig. 2 shows the tissue probability maps of different tissue types calculated from 150 normal adult MR brain images obtained from the ADNI dataset.

3. RESULTS

Two sets of experiments were carried out to evaluate the proposed 4-D image segmentation algorithm. In the first experiment, we used simulated serial MR brain data where the ground truth of the segmentations is known. In the second experiment serial MR brain image data from the ADNI study were used for calculating the longitudinal measures.

3.1 Experiments on Simulated Longitudinal Data

The proposed algorithm is validated first on simulated images.¹⁵ The images are simulated as follows. A statistical model is first trained using the 3-D registration results obtained from 150 ADNI MR brain data and then used to simulate a number of new deformation fields from a given template image, to synthesize MR brain images of different subjects. Serial images are simulated for each simulated subject image by using the atrophy simulation package. Thus each simulated subject consists of longitudinal atrophy in their serial images. Notice we simulated the segmented images first and then added spatially correlated Gaussian noises to them, where the mean intensities of WM, GM and CSF are 110, 85 and 45, respectively, and the standard deviation of the Gaussian noise is 15. In this way, the ground truth of the tissue types of these serial images and the longitudinal deformations of the serial images are known.

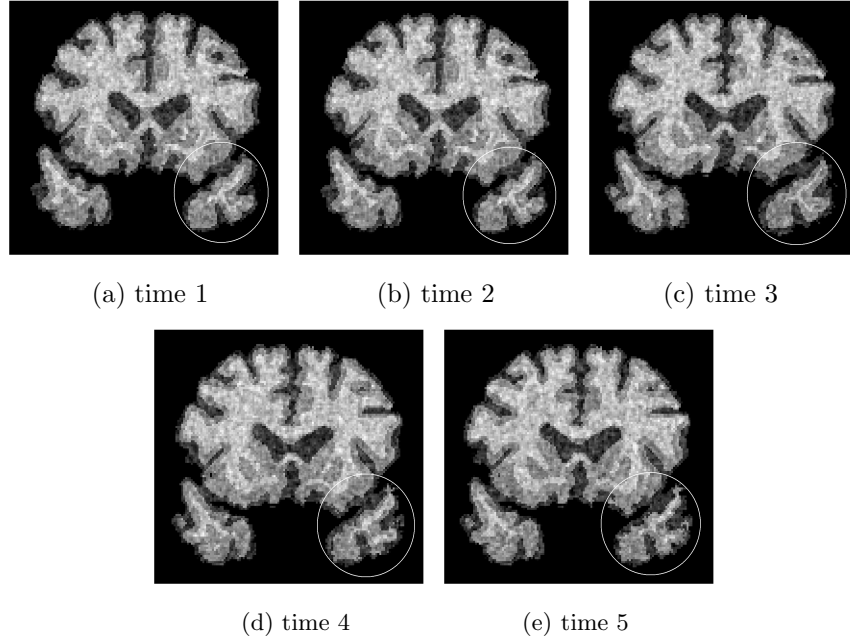


Figure 5. A series of simulated images with atrophy on the temporal lobe.

Fig. 3 shows the template image and its segmentation image randomly selected from the dataset. Fig. 4 shows three examples of the simulated images. The first row gives three warped template images using the simulated deformation fields, and the second row gives the corresponding warped segmentation images. It can be seen that using the statistical model-based deformation simulation,¹⁵ various realistic anatomical shapes of MR brain images can be simulated. The longitudinal data are generated by first manually selecting a point within the temporal lobe and then simulating a gradual atrophy of a spherical region around that point across with time. For each subject image, five images are simulated, and Fig. 5 gives an example of the simulated serial images.

After generating the simulated images, the proposed 4-D segmentation algorithm is evaluated with (CLASSIC-I) and without (CLASSIC-II) the tissue probability map constraints by segmenting these datasets. The correct classification rate (CCR) can be calculated for each segmentation result with respect to the ground truth to evaluate the performance of the proposed algorithm. Fig. 6 shows the CCR for different subjects across different timepoints. We can see more accurate segmentation by applying the tissue probability map constraints in the 4-D fuzzy clustering algorithm.

3.2 Experiments on Longitudinal Images of Alzheimer's Disease

We also applied the proposed algorithm to ADNI (www.loni.ucla.edu) data. The primary goal of ADNI has been to test whether serial magnetic resonance imaging (MRI), positron emission tomography (PET), other biological markers, and clinical and neuropsychological assessment can be combined to measure the progression of mild cognitive impairment (MCI) and early Alzheimer's disease (AD). In this preliminary experiment, we applied the algorithm to 30 ADNI datasets (MCI), and the goal is to evaluate the performance of the algorithm on real data. For all the original MR brain data, the FSL BET skull stripping program has been used to remove the skulls, and some manual corrections were conducted for larger skulls that have not been removed. Then the proposed 4-D segmentation algorithm was used to segment these serial images.

In order to quantitatively analyze the segmentation results, we used a temporal consistency (TC) factor to calculate the temporal consistency of the segmentation results. Suppose $x_{(t,i)}^{\text{seg}}$ is the segmentation result (label) of voxel $x_{(t,i)}$, the segmentation results of voxel $x_{(t,i)}$ across different timepoints can be denoted as $x_{(t_1,i)}^{\text{seg}}, x_{(t_2,i)}^{\text{seg}}, \dots, x_{(t_Y,i)}^{\text{seg}}$. Denote L_i as the number of label changes of the corresponding voxels across different times, the

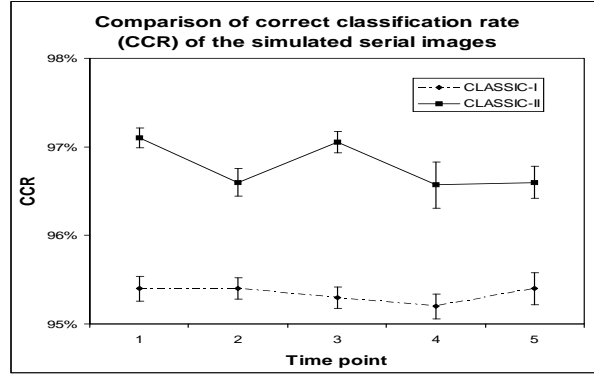


Figure 6. The correct classification rates (CCR) for all the simulated image series.

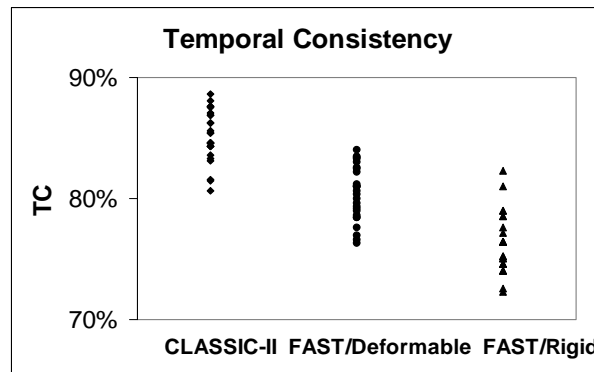


Figure 7. The temporal consistency of the whole brain of all the subjects using different segmentation algorithms.

segmentation is temporally consistent if L_i is small, and vice versa. Therefore, the TC of segmentation results of the image series can be measured by $TC = 1/S(\Omega') \sum_{i \in \Omega'} (1 - L_i / (Y - 1))$, where Ω' is the voxel set of the region of interest, and $S(\Omega')$ is the number of voxels in Ω' .

Both the TC values obtained from a 3-D segmentation, FAST,¹⁸ and CLASSIC-II are calculated and shown in Fig. 7. Notice that the longitudinal deformations among the serial images are needed in order to calculate the TC values. For the 3-D segmentation results, we applied two kinds of registration to get them, namely the FSL FLIRT affine registration¹⁸ and the 3-D hierarchical volumetric image registration.¹⁷ For CLASSIC-II, both the longitudinal deformations and the 4-D segmentation results can be obtained simultaneously. Fig. 7 indicates the TC values for 4-D algorithm are much higher than those of 3-D, indicating that longitudinally stable segmentation and alignment of serial images is achieved. Thus the proposed algorithm yields relative stable temporal morphological measures as compared to the previous algorithms. In the future work, we plan to further evaluate and apply the algorithm in follow up studies of neurological disease.

4. CONCLUSION

This paper proposed a tissue probability map constrained 4-D image segmentation algorithm for longitudinal image analysis. The algorithm iteratively estimates the longitudinal deformations among the image series that reflect the underlying structural changes across time and jointly segments the serial images. By using the tissue probability map as an additional constraint in the clustering algorithm, more accurate and robust segmentation results can be obtained for serial images. Experiments with simulated MR brain images and the ADNI data have confirmed the advantages of this algorithm.

5. ACKNOWLEDGEMENT

The authors would like to thank ADNI for sharing the data (www.loni.ucla.edu/ADNI). As such, the investigators within the ADNI contributed to the design and implementation of ADNI and/or provided data but did not participate in analysis or writing of this report. ADNI investigators include (complete listing available at www.loni.ucla.edu/Collaboration/ADNI_Manuscript_Citations.pdf).

REFERENCES

- [1] Bezdek, J., Hall, L., and Clarke, L., "Review of MR image segmentation techniques using pattern recognition," *Medical Physics* **20**(4), 1033–1048 (1993).
- [2] Chen, W. and Giger, M., "A fuzzy c-mean (FCM) based algorithm for intensity inhomogeneity correction and segmentation of MR images," in [*IEEE International Symposium on Biomedical Imaging (ISBI 2004)*], 1307–1310, Arlington, VA (2004).
- [3] Rezaee, M., van der Zwet, P., , Lelieveldt, B., van der Geest, R., and Reiber, J., "A multiresolution image segmentation technique based on pyramidal segmentation and fuzzy clustering," *IEEE Trans. on Image Processing* **9**(7), 1238–1248 (2000).
- [4] Tang, Y., Whitman, G., Lopez, I., and Baloh, R., "Brain volume changes on longitudinal magnetic resonance imaging in normal older people," *Journal of Neuroimaging* **11**(4), 393–400 (2001).
- [5] Shen, D. and Davatzikos, C., "Measuring temporal morphological changes robustly in brain MR images via 4-D template warping," *NeuroImage* **21**(4), 1508–1517 (2004).
- [6] Wang, F. and Vemuri, B., "Simultaneous registration and segmentation of anatomical structures from brain MRI," in [*MICCAI 2005*], Palm Springs, CA, Springer (2005).
- [7] Chen, X., Brady, M., Lo, J., and Moore, N., "Simultaneous segmentation and registration of contrast-enhanced breast MRI," in [*IPMI 2005*], Glenwood Springs, CO, Springer (2005).
- [8] Ayvaci, A. and Freedman, D., "Joint segmentation-registration of organs using geometric models," *Conf Proc IEEE Eng Med Biol Soc* **2007**, 5251–4 (2007).
- [9] Droske, M. and Rumpf, M., "Multiscale joint segmentation and registration of image morphology," *IEEE Trans Pattern Anal Mach Intell* **29**(12), 2181–94 (2007).
- [10] Pohl, K. M., Fisher, J., Grimson, W. E., Kikinis, R., and Wells, W. M., "A bayesian model for joint segmentation and registration," *Neuroimage* **31**(1), 228–39 (2006).
- [11] Wang, F., Vemuri, B. C., and Eisenschenk, S. J., "Joint registration and segmentation of neuroanatomic structures from brain mri," *Acad Radiol* **13**(9), 1104–11 (2006).
- [12] Wyatt, P. P. and Noble, J. A., "Map mrf joint segmentation and registration of medical images," *Med Image Anal* **7**(4), 539–52 (2003).
- [13] Xue, Z., Shen, D., and Davatzikos, C., "Classic: consistent longitudinal alignment and segmentation for serial image computing," *Neuroimage* **30**(2), 388–99 (2006).
- [14] Pham, P. and Prince, J., "Fantasm: Fuzzy and noise tolerant adaptive segmentation method," in [<http://iacl.ece.jhu.edu/projects/fantasm/>], (www).
- [15] Xue, Z., Shen, D., Karacali, B., Stern, J., Rottenberg, D., and Davatzikos, C., "Simulating deformations of mr brain images for validation of atlas-based segmentation and registration algorithms," *NeuroImage* **33**(3), 855–866 (2006).
- [16] Yan, M. and Karp, J., "An adaptive bayesian approach to three-dimensional MR image segmentation," in [*the Conference on Information Process in Medical Imaging*], (1995).
- [17] Shen, D. and Davatzikos, C., "HAMMER: Hierarchical attribute matching mechanism for elastic registration," *IEEE Transactions on Medical Imaging* **21**(11), 1421–1439 (2002).
- [18] FSL, "Fmrib software library," in [<http://www.fmrib.ox.ac.uk/fsl/index.html>], (www).